Multichannel microwave photonic based direction finding system

Huang, Chongjia; Chan, Erwin

Published in:
Optics Express

DOI:
10.1364/OE.397968

Published: 17/08/2020

Document Version
Publisher's PDF, also known as Version of record

Research Article | Vol. 28, No. 17 / 17 August 2020 / Optics Express 25346

Optics EXPRESS

Multichannel microwave photonic based direction finding system

CHONGJIA HUANG AND ERWIN H. W. CHAN*

College of Engineering, IT and Environment, Charles Darwin University, Darwin NT 0909, Australia
*erwin.chan@cdu.edu.au

Abstract: A new microwave photonic topology for RF signal direction finding is presented. It is based on a dual-parallel Mach Zehnder modulator (DPMZM) in series with an optical phase modulator (PM). The direction of an RF signal received by the antennas connected to an RF port of the DPMZM and the PM can be determined from the power ratio of two system output low frequency components, without the need to know the incoming RF signal amplitude in advance. The proposed structure is suitable for implementing a long baseline technique for direction finding and can be extended to have multiple antenna elements in remote locations. In addition to direction finding, the system also has the ability to measure an RF signal Doppler frequency shift to determine an object speed and moving direction when it is used in a radar receiver. Results obtained using the proposed structure demonstrate less than ±2.5° errors over a 3.2° to 81.5° angle of arrival measurement range for different RF signal modulation indexes of 0.02, 0.08 and 0.16. Doppler frequency shift measurement with less than 0.8 Hz errors is also demonstrated.

1. Introduction

Direction finding (DF) is the measurement of the direction from which a received signal was transmitted. It is used in navigation of ships and aircrafts, to locate emergency transmitters for search and rescue, and to locate the position of emery transmitters. A DF antenna is often a phased array antenna (PAA) made of two or more elements that are physically displaced from each other. The phase difference of the RF signal received by two array elements contains information on the angle of the RF signal arrived at the PAA, which can be used to determine the transmitter location. Precision of the angle of an RF signal arrived at the antenna can be increased by increasing the array element separation or the antenna baseline length [1,2]. Hence, many electronic warfare receiver systems use a long baseline technique for DF where the array elements are separated by approximately 30 m [3]. RF signal transmission in long baseline DF systems is often implemented using microwave photonic links to have less frequency-dependent loss compared to using coaxial links. Since the RF signal is already in the optical domain, it is sensible to implement the DF operation in the optical domain. Microwave photonic based DF systems also have advantages of electromagnetic interference immunity, light weight and small size.

DF systems based on a dual-drive Mach Zehnder modulator (DDMZM) [4,5] or a dual-parallel Mach Zehnder modulator (DPMZM) [6–8] where the RF ports of the modulator are connected to two array elements of a PAA for receiving RF signals, cannot be used to realise long baseline DF. They are also not suitable for implementing a DF system with more than two array elements. These limitations can be avoided in DF systems based on a cascaded Mach Zehnder modulator (MZM) configuration [9–11]. The operating point of an MZM needs to be controlled via a bias controller to obtain a long-term stable performance. This increases the system size, weight and power consumption, which causes problems when the MZM is placed in a remote location for long baseline DF.

In this paper, we present a new microwave photonic based DF system. It is based on a DPMZM in series with an optical phase modulator (PM), which is different to the reported cascaded MZM

#397968 https://doi.org/10.1364/OE.397968
Journal © 2020 Received 18 May 2020; revised 1 Jul 2020; accepted 14 Jul 2020; published 12 Aug 2020

Optics EXPRESS

based DF systems [9–11] and has three main advantages. First, no bias controller is needed for the PM installed in the remote location. Second, it eliminates the needs of the incoming RF signal amplitude to be measured or a calibration procedure prior to the angle of arrival (AOA) measurement, which is required for the systems presented in [6,9,11]. Third, the proposed DF system can simultaneously measure the AOA and the Doppler frequency shift (DFS) of an RF signal when it is used in a radar receiver. It can also be extended to a multichannel DF system. The paper is organised as follows. In Section 2, the topology and the operation principle of the proposed DF system is presented. This section also provides the mathematical formulation for the system output powers and the design of the system parameters to obtain an RF signal AOA independent to the incoming RF signal amplitude. Simulation results and discussion on the system performance are given in Section 3. Section 4 presents the experimental results on the proposed system, which demonstrates its abilities of measuring AOA and DFS independent to the incoming RF signal amplitude. Finally, conclusions are presented in Section 5.

2. Topology and operation principle

A multichannel microwave photonic based DF system is depicted in Fig. 1(a). Continuous wave (CW) light from a laser diode is injected into a DPMZM, which consists of two parallel DDMZMs in the two arms of a main MZM. Two microwave signals, where one is an RF signal received by an antenna labelled as Reference Antenna in the figure and the other is generated by a microwave signal source, are applied separately to the two input RF ports of the top DDMZM. The frequency of the source signal is slightly different to the frequency of the RF signal received by the antenna. The top DDMZM is biased at the null point to maximise the modulator output sideband amplitudes. The bottom DDMZM is driven by a local oscillator (LO). The LO has a fixed low frequency of few MHz. The bottom DDMZM is operated under the same working principle as a single sideband (SSB) modulator [12]. Therefore, the output of the DPMZM consists of the optical carrier at f_c, two pairs of sidebands at $f_c \pm f_S$ and $f_c \pm f_{RF}$, and a LO sideband at f_c-f_{LO}, as shown in Fig. 2(a).

The DPMZM output electric field can be written as

$$E_{DPMZM}(t) = \frac{1}{4}\sqrt{t_{ff1}}E_{in}e^{j\omega_c t}\begin{bmatrix} J_0(m_{LO})(1+j)e^{j\alpha} - 2J_1(m_{LO})e^{-j(\omega_{LO}t-\alpha)} \\ +J_0(m_{RF}) + J_1(m_{RF})e^{j\omega_{RF}t} - J_1(m_{RF})e^{-j\omega_{RF}t} \\ -J_0(m_S) - J_1(m_S)e^{j\omega_S t} + J_1(m_S)e^{-j\omega_S t} \end{bmatrix} \quad (1)$$

where t_{ff1} is the insertion loss of the DDMZM, E_{in} is the electric field amplitude of the CW light, ω_c=2πf_c, ω_S=2πf_S, ω_{RF}=2πf_{RF} and ω_{LO}=2πf_{LO} are the angular frequency of the optical carrier, the source signal, the RF signal and the LO respectively, α is the main MZM bias angle, $J_n(x)$ is the n-th order Bessel function of the first kind, m_S=πV_S/$V_{\pi,DDMZM}$, m_{RF}=πV_{RF}/$V_{\pi,DDMZM}$ and m_{LO}=πV_{LO}/$V_{\pi,DDMZM}$ are the source signal, RF signal and LO modulation index respectively, V_S, V_{RF} and V_{LO} are the voltage of the source signal, the RF signal and the LO respectively, and $V_{\pi,DDMZM}$ is the DDMZM switching voltage. The modulated optical signal at the output of the DPMZM is equally split to three optical signals via an optical coupler for implementing a DF system with four array elements [10]. Each of the three optical signals is injected into a PM driven by the RF signal received by an antenna. Note that each of the PM-antenna pair can be placed in a different remote location for RF signal DF using a long baseline technique. As an example, the system shown in Fig. 1(a) can be installed in an aircraft [2,3] where the PM-antenna pairs are placed on the wingtips and the tail of an aircraft, and the DPMZM-antenna pair is placed at the nose of an aircraft. Signal detection and processing are performed by a centrally located receiver.

Optics EXPRESS

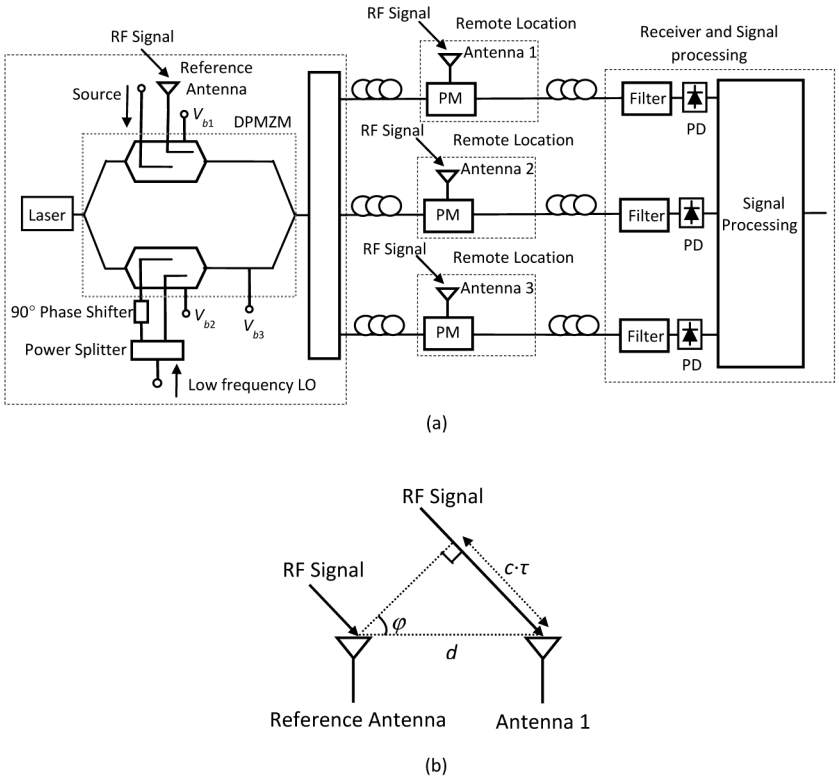

Fig. 1. (a) Schematic diagram of the proposed microwave photonic based DF system. (b) RF signal incident on two array elements.

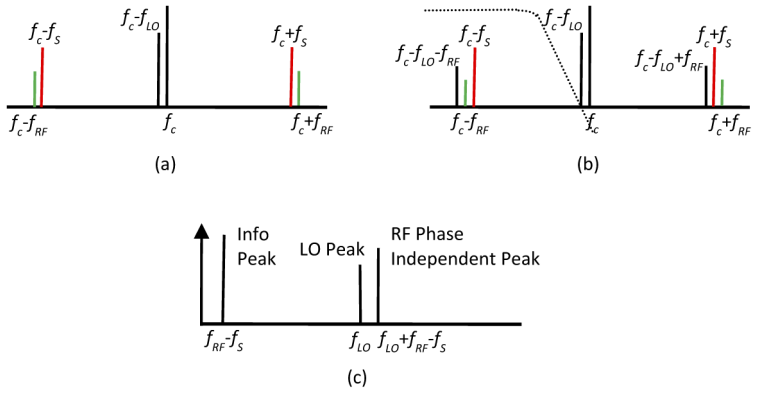

Fig. 2. Optical spectrum at the output of (a) the DPMZM and (b) the PM. The dotted line is the optical filter amplitude response. (c) System output electrical spectrum. f_c, f_S, f_{RF} and f_{LO} are the frequency of the carrier, source signal, incoming RF signal and low-frequency LO respectively.

Optics EXPRESS

The electric field at the output of a PM can be expressed as

$$E_{PM}(t) = \tfrac{1}{4}\sqrt{t_{ff_1}t_{ff_2}}E_{in}e^{j\omega_c t}[J_0(m_{RF}) + J_1(m_{RF})e^{j(\omega_{RF}t+\theta)} - J_1(m_{RF})e^{-j(\omega_{RF}t+\theta)}] \times \begin{bmatrix} J_0(m_{LO})(1+j)e^{j\alpha} - 2J_1(m_{LO})e^{-j(\omega_{LO}(t+\tau)-\alpha)} \\ +J_0(m_{RF}) + J_1(m_{RF})e^{j\omega_{RF}(t+\tau)} - J_1(m_{RF})e^{-j\omega_{RF}(t+\tau)} \\ -J_0(m_S) - J_1(m_S)e^{j\omega_S(t+\tau)} + J_1(m_S)e^{-j\omega_S(t+\tau)} \end{bmatrix} \quad (2)$$

where t_{ff2} is the insertion loss of the PM, τ is the signal time delay introduced by the separation between the DPMZM and the PM, and θ is the phase difference of the RF signal into the PM relative to that into the DPMZM. Assuming the PM has the same switching voltage as the DPMZM for simplicity. Thus, the RF signal modulation index in the PM and the DPMZM are the same. Figure 2(b) shows the optical spectrum at the output of the PM. Note that the sidebands at f_c-f_{LO}±f_{RF} is generated by RF signal modulation on the LO sideband in the PM. Also note that the optical carrier is modulated by an RF signal twice where one is at the DPMZM and the other is at the PM. Since the RF signal into the DPMZM and the PM are received by different antennas, they might have a different phase depending on the AOA of the RF signal. The relationship between the AOA φ and the phase difference θ of the RF signal received by two antennas can be obtained using trigonometric function in the triangle shown in Fig. 1(b). It is given by

$$\varphi = \sin^{-1}\left(\frac{c\cdot\theta}{2\pi f_{RF}\cdot d}\right) \quad (3)$$

where c is the speed of light in vacuum and d is the distance between two antennas. An optical filter, which has an amplitude response as shown by the dotted line in Fig. 2(b), is connected after the PM. It filters out the upper sidebands, the optical carrier and the LO sideband. This leaves three lower sidebands at f_c-f_{LO}-f_{RF}, f_c-f_{RF} and f_c-f_S to be detected by a low-speed photodetector (PD). The electric field into the PD is given by

$$E_{out}(t) = \frac{1}{4}\sqrt{t_{ff_1}t_{ff_2}}E_{in}e^{j\omega_c t}\begin{bmatrix} -[J_0(m_{LO})(1+j)e^{j\alpha} + J_0(m_{RF}) - J_0(m_S)]J_1(m_{RF})e^{-j(\omega_{RF}t+\theta)} \\ -J_0(m_{RF})J_1(m_{RF})e^{-j\omega_{RF}(t+\tau)} + J_0(m_{RF})J_1(m_S)e^{-j\omega_S(t+\tau)} \\ +2J_1(m_{LO})J_1(m_{RF})e^{-j(\omega_{LO}(t+\tau)-\alpha)}e^{-j(\omega_{RF}t+\theta)} \end{bmatrix} \quad (4)$$

Beating of these sidebands at the PD produces three low-frequency components as shown in Fig. 2(c). The frequency components at f_{RF}-f_S and f_{LO}, which are labelled as the info peak and the LO peak in Fig. 2(c), are generated by the beating of the RF signal sideband at f_c-f_{RF} with the sidebands at f_c-f_S and f_c-f_{LO}-f_{RF} respectively. Their powers can be obtained from (4) and are given by

$$P_{Info} = \tfrac{1}{64}t_{ff_1}^2t_{ff_2}^2P_{in}^2J_0^2(m_{RF})J_1^2(m_{RF})J_1^2(m_S)\Re^2R_o \times \begin{bmatrix} \left(\sqrt{2}J_0(m_{LO}) - J_0(m_S)\right)^2 + 2(J_0(m_{RF}) - J_0(m_S))J_0(m_{RF})(\cos(\omega_{RF}\tau - \theta) + 1) \\ +2\sqrt{2}(J_0(m_{RF}) - J_0(m_S))J_0(m_{LO})\left(\cos(\alpha + \tfrac{\pi}{4}) - 1\right) \\ 2\sqrt{2}J_0(m_{RF})J_0(m_{LO})\left(\cos(\omega_{RF}\tau - \theta + \alpha + \tfrac{\pi}{4}) + 1\right) \end{bmatrix} \quad (5)$$

Optics EXPRESS

$$P_{LO} = \frac{1}{16} t_{ff_1}^2 t_{ff_2}^2 P_{in}^2 J_1^2(m_{LO}) J_1^4(m_{RF}) \Re^2 R_o \times \begin{bmatrix} \left(\sqrt{2}J_0(m_{LO}) - J_0(m_S)\right)^2 + 2(J_0(m_{RF}) - J_0(m_S))J_0(m_{RF})(\cos(\omega_{RF}\tau - \theta) + 1) \\ +2\sqrt{2}(J_0(m_{RF}) - J_0(m_S))J_0(m_{LO})\left(\cos(\alpha + \frac{\pi}{4}) - 1\right) \\ 2\sqrt{2}J_0(m_{RF})J_0(m_{LO})\left(\cos(\omega_{RF}\tau - \theta + \alpha + \frac{\pi}{4}) + 1\right) \end{bmatrix} \quad (6)$$

where P_{in} is the power of the CW light from the laser diode, and $\Re$ and R_o are the responsivity and the load resistance of the PD respectively. It can be seen from (5) and (6) that the power of both the info peak and the LO peak are dependent on the phase difference of the RF signal received by two antennas. This shows the RF signal phase difference is translated into change in the info and LO peak powers. Equations (5) and (6) also show the info and LO peak powers are proportional to ${J_1}^2(m_{RF})$ and ${J_1}^4(m_{RF})$ respectively. Hence, they are dependent on the incoming RF signal amplitude. The frequency component at f_{LO}+f_{RF}-f_S in Fig. 2(c) is generated by the beating of the sidebands at f_c-f_{LO}-f_{RF} and f_c-f_S. Its power is given by

$$P_{Indep} = \frac{1}{16} t_{ff_1}^2 t_{ff_2}^2 P_{in}^2 J_1^2(m_{LO}) J_1^2(m_{RF}) J_0^2(m_{RF}) J_1^2(m_S) \Re^2 R_o \quad (7)$$

Equation (7) shows the power of the frequency component at f_{LO}+f_{RF}-f_S is independent to the RF signal phase difference and hence it is referred to as the RF phase independent peak. Note that, as the info peak, the power of the RF phase independent peak is proportional to ${J_1}^2(m_{RF})$. The term ${J_1}^2(m_{RF})$ is eliminated in the info to RF phase independent peak power ratio, which can be expressed as

$$\frac{P_{Info}}{P_{Indep}} = \frac{1}{4J_1^2(m_{LO})} \begin{bmatrix} \left(\sqrt{2}J_0(m_{LO}) - J_0(m_S)\right)^2 + 2(J_0(m_{RF}) - J_0(m_S))J_0(m_{RF})(\cos(\omega_{RF}\tau - \theta) + 1) \\ +2\sqrt{2}(J_0(m_{RF}) - J_0(m_S))J_0(m_{LO})\left(\cos(\alpha + \frac{\pi}{4}) - 1\right) \\ +2\sqrt{2}J_0(m_{RF})J_0(m_{LO})\left(\cos(\omega_{RF}\tau - \theta + \alpha + \frac{\pi}{4}) + 1\right) \end{bmatrix} \quad (8)$$

Equation (8) can be simplified by biasing the main MZM inside the DPMZM at the peak point, i.e. α=0, and designing the source and LO modulation indexes so that $\sqrt{2}J_0(m_{LO})$=$J_0(m_S)$ and the time delay τ so that

$$\omega_{RF}\tau = \frac{8m - 1}{4}\pi \quad (9)$$

where m is an integer. Hence (8) becomes

$$\frac{P_{Info}}{P_{Indep}} = \frac{1}{2J_1^2(m_{LO})} \left\{ \begin{array}{l} [J_0(m_{RF}) - J_0(m_S)] \cdot \left[\left(1 - \sqrt{2}\right)J_0(m_{LO}) + J_0(m_{RF})\left(\cos\left(\frac{8m-1}{4}\pi - \theta\right) + 1\right)\right] \\ +\sqrt{2}J_0(m_{RF})J_0(m_{LO})(\cos(\theta) + 1) \end{array} \right\} \quad (10)$$

Note that the first term inside the curly brackets in (10) is proportional to $J_0(m_{RF})$-$J_0(m_S)$ and is much smaller than the second term, which is shown in the second line of (10), when the incoming RF signal and the source signal are small signals. This shows, by designing the system parameter values, the info to RF phase independent peak power ratio can be made to be almost independent to the incoming RF signal amplitude. Hence the phase difference θ and consequently the AOA φ of the RF signal can be determined from the power ratio without using a calibration procedure or measuring the incoming RF signal amplitude [6,9,11].

3. Simulation results and discussion

Figure 3 shows the info to RF phase independent peak power ratio obtained using (10) with m_{LO}=1.18 and m_S=0.4, for a different RF signal modulation index ranged from 0.01 to 0.16.

Optics EXPRESS

It can be seen from the figure that the power ratio reduces as the RF signal phase difference increases. Most importantly, the figure shows the power ratio has very little dependence on the RF signal modulation index. For example, it can be seen from Fig. 3(b) that, for a 120° RF signal phase difference, there is only 0.08 dB change in the power ratio when the RF signal modulation index increases from 0.01 to 0.16. Figure 4(a) shows the RF signal AOA obtained from the power ratio versus the actual RF signal AOA for a different RF signal modulation index when the power ratio with a 0.08 RF signal modulation index was used as a reference. Errors in the estimated AOA introduced by changes in the incoming RF signal amplitude is shown in Fig. 4(b). It can be seen from the figure that the errors are within ±1° over an RF signal AOA range of 6.1° to 85.3°.

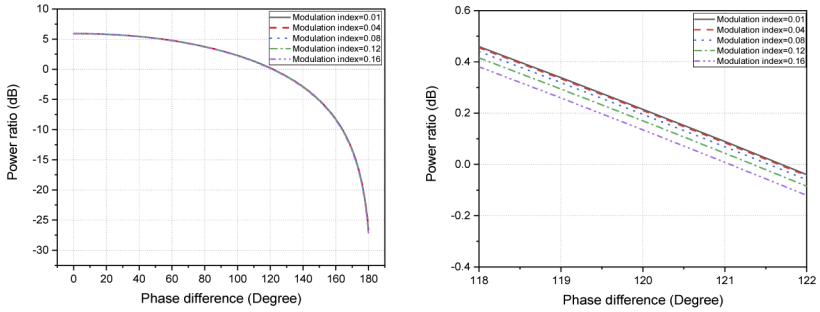

Fig. 3. Simulated info to RF phase independent peak power ratio when the phase difference of the RF signal received by two antennas is changed from (a) 0° to 180° and (b) 118° to 122°.

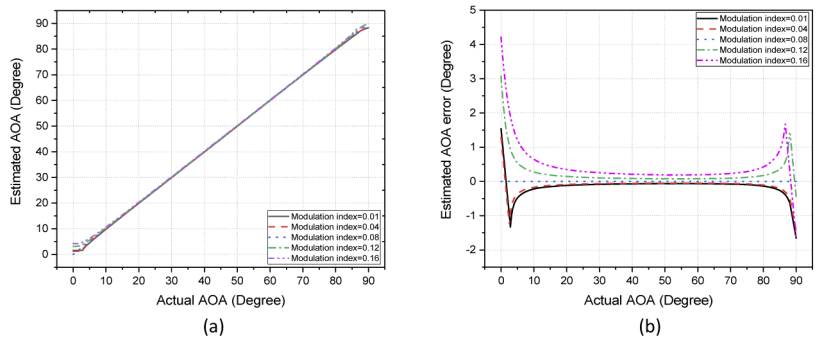

Fig. 4. (a) Estimated RF signal AOA and (b) error in the estimated RF signal AOA versus actual RF signal AOA. The AOA obtained using the power ratio with a 0.08 RF signal modulation index was used as a reference.

Comparing with MZMs, PMs do not require a bias voltage. They can be placed in remote locations without bias drift problem. On the other hand, a bias controller is required for the DPMZM to obtain a long-term stable performance. Recently, a technique to lock a DPMZM at arbitrary bias points has been reported [13] and is suitable for use in the proposed DF system. Note that the frequency of the LO into the proposed structure only needs to be few MHz and is fixed regardless the incoming RF signal frequency. Hence a low-cost low-frequency power splitter and phase shifter can be used at the DDMZM input RF ports to realise SSB modulation. As an example, considering the RF signal and the source signal has 100 kHz frequency difference and the frequency of the LO is 4 MHz. The system output info peak, LO peak and RF phase independent peak are located at 100 kHz, 4 MHz and 4.1 MHz respectively. Only a low-frequency

Optics EXPRESS

electrical spectrum analyser (ESA) is needed to measure the info to RF phase independent peak power ratio to determine the RF signal AOA. The system upper operating frequency is only limited by the optical modulator bandwidth. MZMs with a wide 3-dB bandwidth of over 100 GHz have been demonstrated [14]. The system lower operating frequency is limited by the sharpness of the optical filter amplitude response edge as an optical filter is required for suppressing the carrier and the upper sidebands while passing the lower sidebands. Simulation results show a 20-dB carrier and upper sideband suppression is needed to obtain more than 35 dB changes in the info peak power when the RF signal AOA is changed from 0° to 90°. Hence, the system lower operating frequency is 6.25 GHz for an optical filter has an edge roll-off of 400 dB/nm, which can be realised by commercial low-cost passive optical filters [15] or a silicon photonics optical filter [16].

When the proposed system is used in a radar receiver, it has the ability to simultaneously determine the location and the velocity of a moving object. In this case, the source signal is a copy of the transmitted signal emitted by the radar. The echo signal, which is the transmitted signal reflected by a moving object, is received by the array elements shown in Fig. 1(a). Due to the Doppler effect, the echo signal has a slightly different frequency compared to the transmitted signal. This frequency difference is called the Doppler frequency shift (DFS) and is dependent on the object speed and moving direction. If an object is moving toward to (away from) the radar receiver then the echo signal has a higher (lower) frequency compared to the transmitted signal. The frequency of the info peak at the system output is $|f_{RF}\text{-}f_S|$, which can be used to determine the object speed. The frequency of the RF phase independent peak can be used to determine the object moving direction. When an object is moving toward to (away from) the radar receiver, the RF phase independent peak has a higher (lower) frequency than the LO peak. The object location can be obtained from the AOA of the echo signal using the power ratio of the info peak to the RF phase independent peak as was discussed above.

4. Experimental results

An experiment was set up as shown in Fig. 5 to verify the proposed structure. A 1550.03 nm 10 dBm CW light generated by a tunable laser source (Keysight N7711A) was launched into a DPMZM (Sumitomo T.SBZH1.5-20PD-ADC) via a polarisation controller (PC). A 3 MHz LO generated by a waveform generator was split into two and passed through a low-frequency phase shifter to introduce a 90° phase difference between two LOs before applying them to the bottom DDMZM inside the DPMZM for SSB modulation. A 15 GHz microwave signal was used as the source signal and was applied to one RF port of the top DDMZM inside the DPMZM. A RF signal at 15 GHz + 300 kHz was equally split into two via a power splitter. The RF signals were applied to the top DDMZM and a PM connected after the DPMZM. The effect of changes in the AOA of the incoming RF signal was emulated with a phase shifter after the power splitter. A variable attenuator was used to ensure the RF signal modulation index in the DDMZM and the PM are the same. Note that the power splitter, the variable attenuator and the phase shifter connected to the RF port of the top DDMZM and the PM were only used to demonstrate the proposed DF system. They are not required in the actual system. The switching voltage of the DDMZM was measured to be 5.1 V and 6.3 V at 3 MHz and 15 GHz respectively. The power into the modulator was adjusted so that the modulation index of the LO, source signal and RF signal were 1.24, 0.43 and 0.08 respectively. The output of the PM was connected to a Fourier domain optical signal processor (Finisar WaveShaper 4000), which was programmed to act as an optical filter to filter out the upper sidebands, the LO sideband and the optical carrier. An erbium-doped fibre amplifier (EDFA) was used to compensate for the system loss. This was followed by a 0.5 nm bandwidth optical filter to suppress the amplified spontaneous emission noise. The output optical signal was detected by a PD whose output was connected to an ESA.

Optics EXPRESS

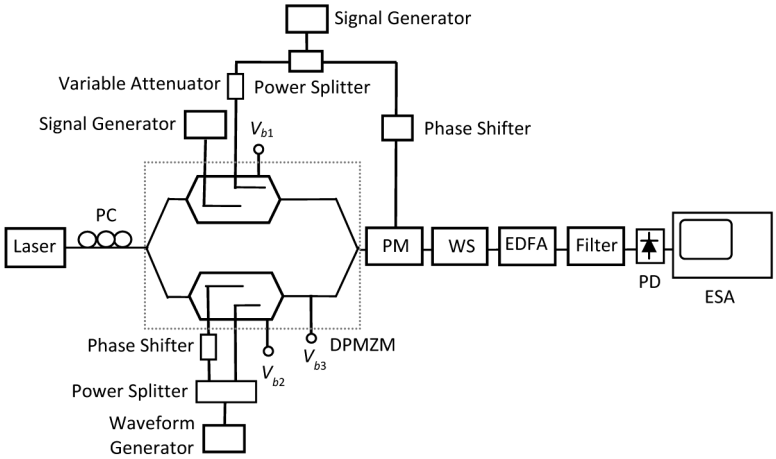

Fig. 5. Experimental setup of the proposed microwave photonic based DF system.

Figures 6(a) and 6(b) show the system output electrical spectrums measured on the ESA when the RF signal into the DPMZM and the PM have a 0° and 150° phase difference respectively. It can be seen from the figure that the frequency of the info peak is 300 kHz, which is the frequency difference between the RF and source signal. The info peak power decreases from −18.6 dBm to −30.7 dBm as the RF signal phase difference increases from 0° to 150°. On the contrary, the power of the RF phase independent peak at 3.3 MHz remains unchanged. Note that slight amplitude and phase imbalance of the LOs into the two RF ports of the bottom DDMZM causes an unwanted sideband at the frequency of f_c+f_{LO} to be presented after the DPMZM. This unwanted sideband into the PM acts as a carrier, just like the wanted sideband at f_c-f_{LO}, which generates a sideband at f_c+f_{LO}-f_{RF}. This sideband passes through the optical filter and beats with the sidebands at f_c-f_s. This produces an unwanted frequency component at 2.7 MHz as shown in Fig. 6. Using a 90° hybrid coupler with a small amplitude and phase imbalance to split the 3 MHz LO can reduce the unwanted frequency component amplitude. Nevertheless, the amplitude of the unwanted frequency component is more than 21 dB below the RF phase independent peak.

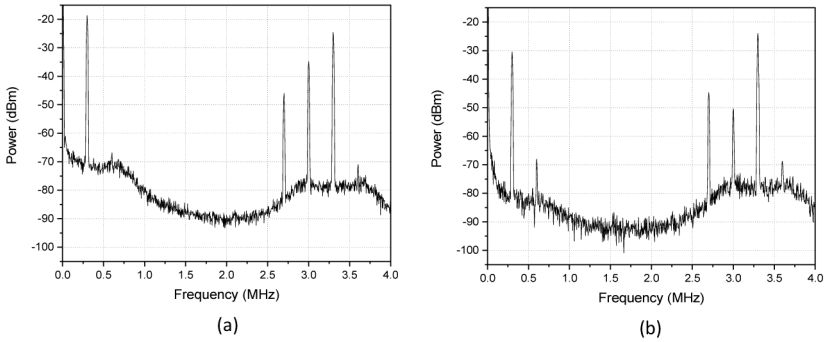

Fig. 6. Measured system output electrical spectrums when a 15 GHz + 300 kHz RF signal into the DPMZM and the PM have a phase difference of (a) 0° and (b) 150°.

Figure 7(a) shows the power of the info peak and the RF phase independent peak for various RF signal phase difference from 0° to 180°. It can be seen from the figure that the info peak power reduces while the RF phase independent peak power remains almost the same, as the RF signal phase difference increases. The figure shows there is a 0.7 dB increase in the RF phase

Optics EXPRESS

independent peak power. This is due to a slight reduction in the total optical power into the EDFA that increases the EDFA gain, as the RF signal phase difference increases. A similar result was obtained for different RF signal modulation indexes of 0.02 and 0.16. Figure 7(b) shows the measured info to RF phase independent peak power ratio versus RF signal phase difference for a different RF signal modulation index of 0.02, 0.08 and 0.16. The figure also shows the simulated power ratio, which was obtained using (10) and the experimental system parameter values. The effect of the input power dependent EDFA gain was included in the simulated power ratio. Excellent agreement between the measurement and theoretical prediction can be seen in Fig. 7(b). The experimental results demonstrate the info to RF phase independent peak power ratio has very little dependence on the input RF signal amplitude.

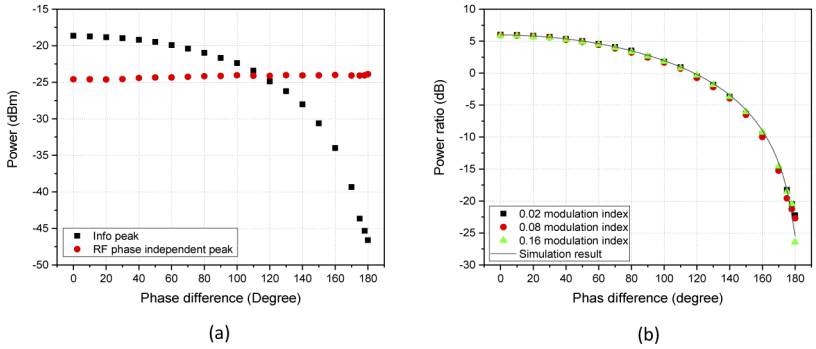

Fig. 7. (a) Measured info peak power (black square) and RF phase independent peak power (red circle) versus the RF signal phase difference for an RF signal modulation index of 0.08. (b) Measured info to RF phase independent peak power ratio at various RF signal phase differences for an RF signal modulation index of 0.02 (black square), 0.08 (red circle) and 0.16 (green triangle), and the simulated power ratio (solid line).

Figure 8(a) shows the estimated AOAs obtained using the measured power ratio shown in Fig. 7(b). AOA measurement errors for 0.02, 0.08 and 0.16 RF signal modulation index, which were obtained by comparing the simulated and measured power ratio, are shown in Fig. 8(b). It can be seen that the errors are within ±2.5° over an AOA range of 3.2° to 81.5° for all three RF signal modulation indexes. This demonstrates the proposed structure is capable to determine the RF signal AOA from the info to RF phase independent peak power ratio without knowing the input RF signal amplitude. Note that both simulation and experimental results in Fig. 4(b) and 8(b) show the errors increase when the RF signal AOA approaches 0° or 90°. However, at 90° RF signal AOA, the measured AOA errors are much larger than the estimated AOA errors. This is because, when the RF signal AOA is 90° which corresponds to the RF signal into the DPMZM and the PM have a 180° phase difference, the info peak amplitude is sensitive to the system parameters such as the EDFA gain and the DPMZM bias points. In the experiment, change in the EDFA gain and drift in the DPMZM bias points alter the info peak amplitude and consequently cause power ratio fluctuation. This results in large errors at 90° AOA compared to the estimated AOA errors shown in Fig. 4(b). Using a modulator bias controller to lock the DPMZM bias points can reduce errors in the measured RF signal AOA.

To further verify the power ratio and consequently the estimated AOA has very little dependence on the amplitude of the input RF signal, the power of the info peak and the RF phase independent peak were measured for a different input RF signal power into the DPMZM. Figure 9 shows the power of the two peaks and the corresponding power ratio when the RF signal into the DPMZM and the PM have 0° phase difference. As expected, the powers of both the info peak and the RF phase independent peak increase linearly with the input RF signal power. There is less than

Optics EXPRESS

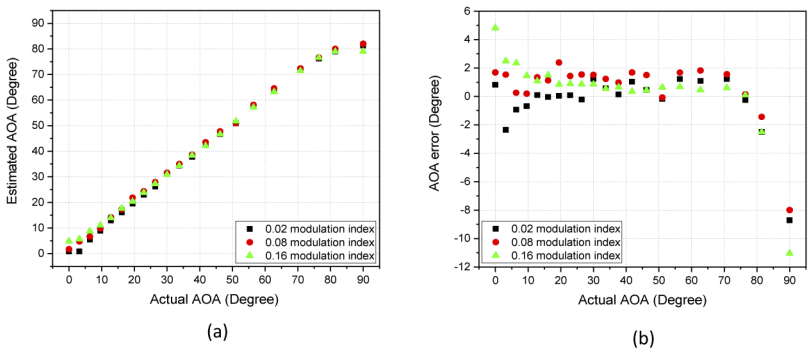

Fig. 8. (a) Estimated AOA versus actual AOA for a 0.02 (black square), 0.08 (red circle) and 0.16 (green triangle) RF signal modulation index. (b) The corresponding AOA measurement error.

0.05 dB change in the ratio of the two peak powers for 18 dB changes in the input RF signal power. This shows that, even in practice the incoming RF signal power is unknown and is changing with time, the RF signal AOA can be determined by simply measuring the info to RF phase independent peak power ratio.

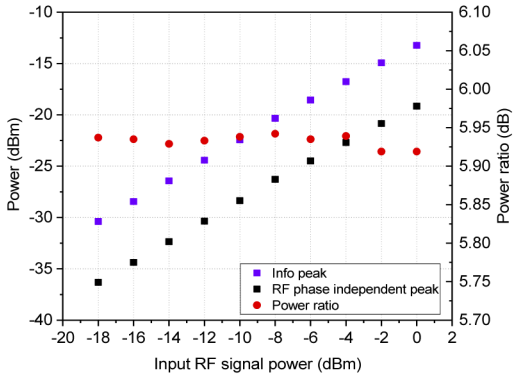

Fig. 9. Measured info peak power (purple square) and RF phase independent peak power (black square) and corresponding power ratio (red circle) for a 0° input RF signal phase difference when the RF signal power into the DDMZM is changed from −18 dBm to 0 dBm.

Finally, in order to verify the proposed structure also has the ability to measure the DFS when it is used in a radar receiver, the frequency of the info peak was measured for a different input RF signal or echo signal frequency. The frequency of the source signal, which is a copy of the microwave signal emitted by the radar, was fixed at 15 GHz. The LO frequency was 3 MHz. Figure 10 shows the DFS and the measurement error, which were obtained by measuring the frequency of the info peak on the system output spectrum and the difference between the info peak frequency and the frequency offset of the input RF and source signal respectively. It can be seen from the figure that the DFS error is less than 0.8 Hz. The system output spectrum also shows the location of the RF phase independent peak changes as the input RF signal frequency changes. The frequency of the RF phase independent peak is larger than the LO peak frequency of 3 MHz, as shown in Fig. 6, when the input RF or echo signal frequency is larger than the source or transmitted signal frequency. This indicates an object is moving toward the radar receiver.

Optics EXPRESS

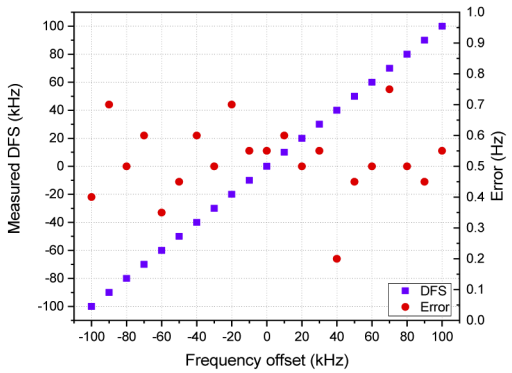

Fig. 10. Measured DFS (purple square) and the corresponding measurement error (red circle) when the frequency of the RF signal is changed from 15 GHz - 100 kHz to 15 GHz + 100 kHz.

5. Conclusion

A cascaded modulator topology for RF signal DF has been presented. The topology comprises a DPMZM, one or more PMs, and an optical filter. It eliminates the limitation of many reported microwave photonic based DF systems, which permits the array elements in a PAA to be placed in multiple different remote locations. This improves the flexibility of PAA installation and the RF signal DF accuracy. The proposal topology can determine the AOA of the incoming RF signal directly from the power ratio of two system output low frequency components, which are the info peak and the RF phase independent peak, without measuring the incoming RF signal amplitude or using a calibration procedure. An experiment has been set up to verify the cascaded modulator topology for RF signal DF. Results have been presented that show excellent agreement between the measured and simulated power ratio at various RF signal phase differences. Less than ±2.5° errors in an RF signal AOA range of 3.5° to 81.5° was obtained for three different input RF signal powers, which correspond to 0.02, 0.08 and 0.16 RF signal modulation indexes. A DFS measurement was also conducted and the results show less than 0.8 Hz errors. The proposed topology should find application in electronic warfare systems that use long baseline technique for DF to enhance the measurement accuracy.

Disclosures

The authors declare no conflicts of interest.

References

1. R. E. Franks, "Direction-finding antennas," in *Antenna Handbook: Volume III Applications*, Y. T. Lo and S. W. Lee, eds., (Springer, 1993).
2. J. Kolanek and E. Carlsen, "Precision geolocation system and method using a long baseline interferometer antenna system," United States Patent, 7286085, 2007.
3. M. E. Manka, "Microwave photonics for electronic warfare applications," *International Topical Meeting on Microwave Photonics*, 275–278 (2008).
4. Z. Cao, Q. Wang, R. Lu, H. P. A. van den Boom, E. Tangdiongga, and A. M. J. Koonen, "Phase modulation parallel optical delay detector for microwave angle-of-arrival measurement with accuracy monitored," Opt. Lett. **39**(6), 1497–1500 (2014).
5. H. Chen and E. H. W. Chan, "Simple approach to measure angle of arrival of a microwave signal," IEEE Photonics Technol. Lett. **31**(22), 1795–1798 (2019).
6. Z. Cao, H. P. A. van den Boom, R. Lu, Q. Wang, E. Tangdiongga, and A. M. J. Koonen, "Angle-of-arrival measurement of a microwave signal using parallel optical delay detector," IEEE Photonics Technol. Lett. **25**(19), 1932–1935 (2013).

Optics EXPRESS

7. H. Zhuo, A. Wen, and Y. Wang, "Photonic angle-of-arrival measurement without direction ambiguity based on a dual-parallel Mach–Zehnder modulator," Opt. Commun. **451**, 286–289 (2019).
8. P. Li, L. Yan, J. Ye, X. Feng, W. Pan, B. Luo, X. Zou, T. Zhou, and Z. Chen, "Photonic approach for simultaneous measurements of Doppler-frequency-shift and angle-of-arrival of microwave signals," Opt. Express **27**(6), 8709–8716 (2019).
9. X. Zou, W. Li, W. Pan, B. Luo, L. Yan, and J. Yao, "Photonic approach to the measurement of time-difference-of-arrival and angle-of-arrival of a microwave signal," Opt. Lett. **37**(4), 755–757 (2012).
10. P. D. Biernacki, R. Madara, L. T. Nichols, A. Ward, and P. J. Matthews, "A four channel angle of arrival detector using optical downconversion," *1999 IEEE MTT-S International Microwave Symposium Digest*, pp. 885–888, (1999).
11. H. Chen and E. H. W. Chan, "Angle of arrival measurement system using double RF modulation technique," IEEE Photonics J. **11**(1), 1–10 (2019).
12. G. H. Smith, D. Novak, and Z. Ahmed, "Novel technique for generation of optical SSB with carrier using a single MZM to overcome fiber chromatic dispersion," *International Topical Meeting on Microwave Photonics*, pp. 5–8, (1996).
13. X. Li, L. Deng, X. Chen, H. Song, Y. Liu, M. Cheng, S. Fu, M. Tang, M. Zhang, and D. Liu, "Arbitrary bias point control technique for optical IQ modulator based on dither-correlation detection," J. Lightwave Technol. **36**(18), 3824–3836 (2018).
14. X. Wang, P. O. Weigel, J. Zhao, M. Ruesing, and S. Mookherjea, "Achieving beyond-100-GHz large-signal modulation bandwidth in hybrid silicon photonics Mach Zehnder modulators using thin film lithium niobate," APL Photonics **4**(9), 096101 (2019).
15. C. Huang, E. H. W. Chan, and C. B. Albert, "A compact photonics-based single sideband mixer without using high-frequency electrical components," IEEE Photonics J. **11**(4), 1–9 (2019).
16. C. Porzi, G. J. Sharp, M. Sorel, and A. Bogoni, "Silicon photonics high-order distributed feedback resonators filters," IEEE J. Quantum Electron. **56**(1), 1–9 (2020).